NASA/TM—2003-212555

SiC Fiber-Reinforced Celsian Composites

Narottam P. Bansal
Glenn Research Center, Cleveland, Ohio

August 2003

The NASA STI Program Office . . . in Profile

Since its founding, NASA has been dedicated to the advancement of aeronautics and space science. The NASA Scientific and Technical Information (STI) Program Office plays a key part in helping NASA maintain this important role.

The NASA STI Program Office is operated by Langley Research Center, the Lead Center for NASA's scientific and technical information. The NASA STI Program Office provides access to the NASA STI Database, the largest collection of aeronautical and space science STI in the world. The Program Office is also NASA's institutional mechanism for disseminating the results of its research and development activities. These results are published by NASA in the NASA STI Report Series, which includes the following report types:

- TECHNICAL PUBLICATION. Reports of completed research or a major significant phase of research that present the results of NASA programs and include extensive data or theoretical analysis. Includes compilations of significant scientific and technical data and information deemed to be of continuing reference value. NASA's counterpart of peer-reviewed formal professional papers but has less stringent limitations on manuscript length and extent of graphic presentations.

- TECHNICAL MEMORANDUM. Scientific and technical findings that are preliminary or of specialized interest, e.g., quick release reports, working papers, and bibliographies that contain minimal annotation. Does not contain extensive analysis.

- CONTRACTOR REPORT. Scientific and technical findings by NASA-sponsored contractors and grantees.

- CONFERENCE PUBLICATION. Collected papers from scientific and technical conferences, symposia, seminars, or other meetings sponsored or cosponsored by NASA.

- SPECIAL PUBLICATION. Scientific, technical, or historical information from NASA programs, projects, and missions, often concerned with subjects having substantial public interest.

- TECHNICAL TRANSLATION. English-language translations of foreign scientific and technical material pertinent to NASA's mission.

Specialized services that complement the STI Program Office's diverse offerings include creating custom thesauri, building customized databases, organizing and publishing research results . . . even providing videos.

For more information about the NASA STI Program Office, see the following:

- Access the NASA STI Program Home Page at ***http://www.sti.nasa.gov***

- E-mail your question via the Internet to help@sti.nasa.gov

- Fax your question to the NASA Access Help Desk at 301–621–0134

- Telephone the NASA Access Help Desk at 301–621–0390

- Write to:
  NASA Access Help Desk
  NASA Center for AeroSpace Information
  7121 Standard Drive
  Hanover, MD 21076

NASA/TM—2003-212555

SiC Fiber-Reinforced Celsian Composites

Narottam P. Bansal
Glenn Research Center, Cleveland, Ohio

National Aeronautics and
Space Administration

Glenn Research Center

August 2003

Acknowledgments

The author would like to thank his collaborators, Dr. Sung Choi, Dr. Jeff Eldridge, Dr. John Gyekenyesi, and Mr. Mark Hyatt (NASA Glenn Research Center), Dr. Özer Ünal (Ames Laboratory), Professor Charles Drummond (OSU), Professor K.P.D. Lagerlof (CWRU), Dr. Rob Dickerson (Los Alamos Laboratory), and Dr. Philippe Colomban (CNRS, France) who made valuable contributions to the Celsian matrix composites project over the last many years. John Setlock, Ralph Garlick, Ron Phillips, Bob Angus, and Ralph Pawlik provided valuable technical assistance during composite fabrication and characterization.

Trade names or manufacturers' names are used in this report for identification only. This usage does not constitute an official endorsement, either expressed or implied, by the National Aeronautics and Space Administration.

The Propulsion and Power Program at
NASA Glenn Research Center sponsored this work.

Available from

NASA Center for Aerospace Information
7121 Standard Drive
Hanover, MD 21076

National Technical Information Service
5285 Port Royal Road
Springfield, VA 22100

Available electronically at http://gltrs.grc.nasa.gov

SiC Fiber-Reinforced Celsian Composites

Narottam P. Bansal
National Aeronautics and Space Administration
Glenn Research Center
Cleveland, Ohio 44135
Phone: 216–433–3855; Email: Narottam.P.Bansal@nasa.gov

Summary

Celsian is a promising matrix material for fiber-reinforced composites for high temperature structural applications. Processing and fabrication of small diameter multifilament silicon carbide tow reinforced celsian matrix composites are described. Mechanical and microstructural properties of these composites at ambient and elevated temperatures are presented. Effects of high-temperature exposures in air on the mechanical behavior of these composites are also given. The composites show mechanical integrity up to ~1100 °C but degrade at higher temperatures in oxidizing atmospheres. A model has been proposed for the degradation of these composites in oxidizing atmospheres at high temperatures.

1. Introduction

Fiber-reinforced ceramic matrix composites are being developed for high-temperature structural applications in aerospace, energy conservation, power generation, nuclear, petrochemical, and other industries. Glasses and glass-ceramics of various compositions (refs. 1 and 2) are being investigated as matrix materials for fiber-reinforced composites. Maximum use temperatures of these matrices in composite form are compared in table 1. Barium aluminosilicate (BAS) glass-ceramic having monoclinic celsian, $BaAl_2Si_2O_8$, as the crystalline phase appears to be the most refractory with a projected maximum use temperature of ~1590 °C and a melting point of 1760 °C. Celsian shows excellent resistance towards oxidation and reduction, has good thermal shock resistance because of its low thermal expansion coefficient, and does not undergo any phase transformation up to ~1590 °C. It also shows reasonably good resistance against alkali attack. It is chemically compatible with various reinforcement materials such as SiC, Si_3N_4, Al_2O_3, and mullite. It shows thermally stable microwave dielectric properties which makes it useful for applications in electromagnetic windows and radomes, microelectronic packaging, and high voltage condensers. Also it is highly effective (refs. 3 and 4) as an environmental barrier coating (EBC) for the protection of SiC_f/SiC combustor liner in the harsh atmosphere of turbine engines. Therefore, celsian is an attractive matrix material for fiber-reinforced composites for applications as high temperature structural materials in hot sections of gas turbine engines. Celsian composites reinforced with small diameter multifilament tow SiC fibers are described here. Processing and properties of large CVD SiC filament reinforced celsian matrix composites are reported elsewhere (refs. 5 to 11).

Table 1.—Glass and glass-ceramic matrices of interest for fiber-reinforced composites (refs. 1 and 2)

Matrix type	Major constituents	Minor constituents	Major crystalline phases	Maximum use temperature in composite form, °C
Glasses[a]				
7740 Borosilicate	B_2O_3, SiO_2	Na_2O, Al_2O_3	--	600
1723 Aluminosilicate	Al_2O_3, MgO, CaO, SiO_2	B_2O_3, BaO	--	700
7930 High silica	SiO_2	B_2O_3	--	1150
Glass-ceramics				
LAS–I	Li_2O, Al_2O_3, MgO, SiO_2,	ZnO, ZrO_2, BaO	β-spodumene	1000
LAS–II	Li_2O, Al_2O_3, MgO, SiO_2, Nb_2O_5	ZnO, ZrO_2, BaO	β-spodumene	1100
LAS–III	Li_2O, Al_2O_3, MgO, SiO_2, Nb_2O_5	ZrO_2	β-spodumene	1200
MAS	MgO, Al_2O_3, SiO_2	BaO	Cordierite	1200
BMAS	BaO, MgO, Al_2O_3, SiO_2	--	Barium osumilite	1250
Ternary mullite	BaO, Al_2O_3, SiO_2	--	Mullite	~1500
Celsian	BaO, Al_2O_3, SiO_2	--	Celsian	~1600

[a]7740, 1723, and 7930 are Corning Glass Works designations

2. Polymorphs and Crystal Structure of Celsian

Celsian (monoclinic space group I2/c) can exist in three different forms: monoclinic, hexagonal and orthorhombic. Hexacelsian (space group P6/mmm) is the high temperature polymorph and is thermodynamically stable above 1590 °C, but once formed can metastably exist in the entire temperature range down to room temperature (fig. 1) (refs. 12 and 13). The kinetics of transformation of hexacelsian into monoclinic celsian is very sluggish (ref. 14). Hexacelsian shows a large thermal expansion coefficient of $\sim 8.0\times10^{-6}$/°C and undergoes a rapid, reversible structural transformation into the orthorhombic form at ~300 °C, accompanied by a large volume change of ~3 percent. In the presence of hexacelsian, thermal cycling of the composite would result in microcracking of the BAS matrix. Obviously, if BAS is to be successfully used as a matrix material for fiber reinforced composites, the processing conditions need to be designed to completely eliminate the undesirable hexacelsian phase.

The crystal structure of hexacelsian (figs. 2 and 3(a)) (ref. 15) contains infinite two-dimensional hexagonal sheets, consisting of two layers of silica tetrahedral sharing all four vertices with substitution of Al for Si and charge compensation by Ba between the sheets. It has been suggested (ref. 16) that the transformation at 300 ºC between orthorhombic and hexagonal forms of hexacelsian involves rotation of these sheets with respect to each other. However, according to Takeuchi (ref. 16), no significant differences are observed between the powder XRD patterns of the orthorhombic and hexagonal forms of hexacelsian except peak shifts owing to lattice expansion, indicating similar fundamental frameworks of both structures.

The celsian structure (fig. 3(b)) (ref. 17) is similar to the feldspar structure in which all four vertices of the silica tetrahedral are shared, forming a three-dimensional network. As in hexacelsian, Al substitutes for Si with charge compensation by Ba in the larger interstices of the structure. Gay (ref. 18) and Newnham and Megaw (ref. 17) considered the formation of a superlattice in celsian associated with ordering of the Al-Si atoms.

In celsian crystal structure (ref. 19) the Al and Si atoms are statistically distributed over tetrahedral sites, so that each Al tetrahedron is surrounded by four predominantly Si tetrahedral and vice versa. The feature of the hexacelsian structure, however, is the presence of $(Al,Si)O_4$ tetrahedra which share three corners so that a hexagonal sheet results with the remaining apices pointing in the same direction. Two of these sheets share their apical oxygens, forming a double tetrahedral sheet (fig. 3(a)). Ba atoms occupy positions between the double sheets with twelve equidistant oxygen neighbors. In celsian, Ba ion has an irregular configuration, so that it has ten oxygen neighbors at several Ba-O distances. Consequently, to transform hexacelsian to celsian would require creation of a three-dimensional network from the two-dimensional sheet structure of hexacelsian as well as rearrangement of the Ba sites. This would entail breaking and reforming of Al-O and Si-O bonds. Some of the physical, mechanical and thermal properties of celsian are given in table 2 (refs. 20 to 22).

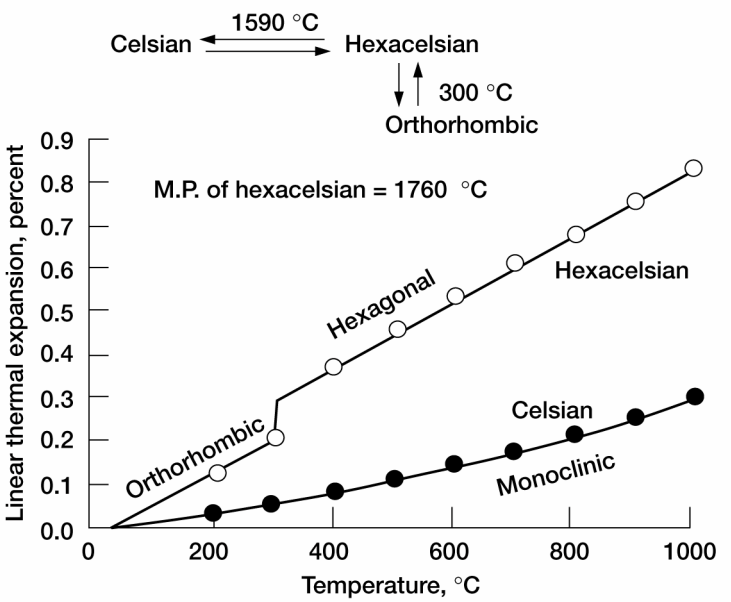

Figure 1.—Linear thermal expansion of hexacelsian and monoclinic celsian BAS.

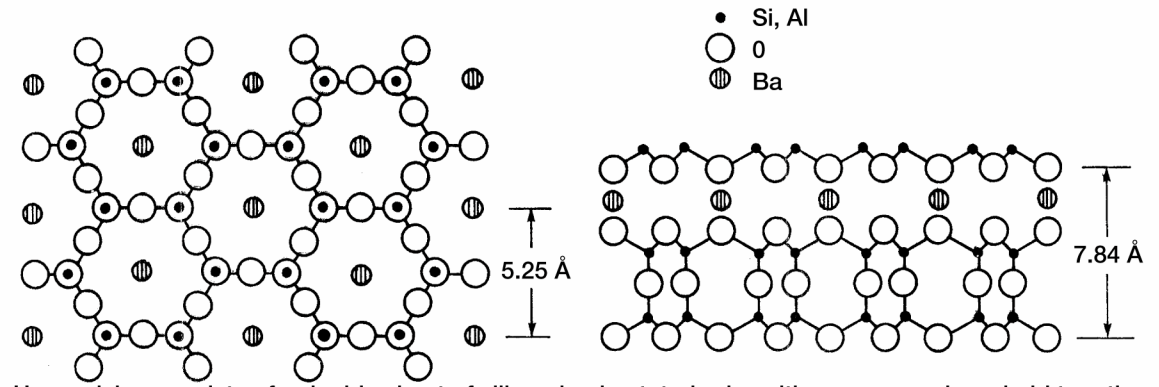

Hexacelsian consists of a double sheet of silica-alumina tetrahedra with common apices, held together by barium ions in 12-fold coordination.

Figure 2.—Structure of hexagonal $BaAl_2Si_2O_8$.

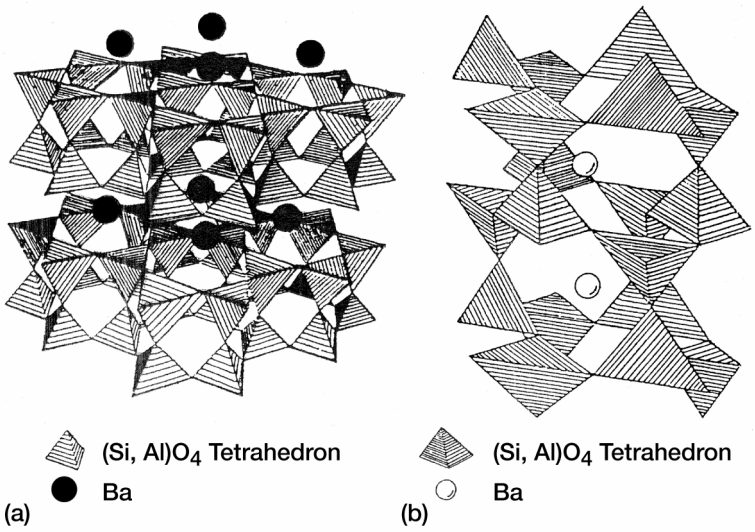

Figure 3.—Crystal structures of (a) hexagonal and (b) monoclinic celsian $BaAl_2Si_2O_8$.

Table 2.—Properties of celsian

Property	Temperature	Value
Melting point, °C	--	1760
Density, g/cm^{-3}	RT	3.39 (monoclinic celsian) 3.26 (hexacelsian)
CTE, $°C^{-1}$	20 to 1000 °C 300 to 1000 °C	2.29×10^{-6} (monoclinic celsian) 8×10^{-6} (hexacelsian)
Flexure modulus, GPa	RT 538 °C 815 °C 1093 °C	100 ± 7 102 ± 14 94 ± 8 87 ± 6
Poisson's ratio	RT	0.32
Flexure (4-point) strength, MPa	RT 500 °C 750 °C 1000 °C 1200 °C 1350 °C	115 ± 15 120 ± 5 100 ± 10 60 ± 5 25 ± 5 25 ± 5
Fracture toughness, $MPa/m^{1/2}$	RT	1.56
Thermal diffusivity, cm^2s^{-1}	RT	0.0114
Heat capacity, $Jg^{-1}K^{-1}$	RT 260 °C 538 °C 815 °C 1093 °C 1372 °C	0.84 0.79 0.88 0.88 0.94 1.02
Thermal conductivity, $Wm^{-1}K^{-1}$	RT 500 °C 1000 °C 1400 °C	3.25 3.1 3.0 2.9

3. Formation of Monoclinic Celsian

On heat treatment, both hexacelsian and monoclinic celsian phases crystallize in BAS glass (refs. 23 to 25). Also, hot pressing of barium aluminosilicate (BAS) glass or its composites reinforced with large diameter silicon carbide SCS-6 monofilaments or small diameter multifilament Nicalon or Hi-Nicalon fibers resulted in the crystallization of both hexacelsian and monoclinic celsian phases (ref. 12). On doping BAS with 5 wt.% monoclinic celsian seeds or 10 wt.% strontium aluminosilicate (SAS), only the celsian phase was formed in hot pressed monolithic specimens. However, in fiber-reinforced composites hot pressed under similar conditions, a small concentration of hexacelsian was still present as hexacelsian nucleates preferentially on the surface and the presence of fibers provides a large surface area. When the additive concentration increased to 10 wt.% celsian seeds or 20 wt.% SAS, celsian was the only phase detected from x-ray diffraction, with complete elimination of hexacelsian, in the hot pressed composites reinforced with SiC fibers. Hence BAS with 20 to 25 percent of SAS was used as the matrix for fiber-reinforced composites.

4. CMC Processing

Ceramic grade Nicalon or Hi-Nicalon fiber tows were used as the reinforcement. Fibers having a dual surface layer of BN overcoated with SiC were used. BN acts as a weak, crack deflecting, compliant layer, while the SiC overcoat acts as a barrier to diffusion of boron from BN into the oxide matrix and also prevents diffusion of matrix elements into the fiber.

The matrix of $0.75BaO\text{-}0.25SrO\text{-}Al_2O_3\text{-}2SiO_2$ (BSAS) composition was synthesized (ref. 20) by a solid-state reaction method from $BaCO_3$, $SrCO_3$, Al_2O_3, and SiO_2 powders. The mixed powder was calcined at ~900 to 910 °C for decomposition of the carbonates. The resulting powder consisted of mainly SiO_2 (α-quartz) and $BaAl_2O_4$ phases with small amounts of Ba_2SiO_4, α-Al_2O_3, and $Ba_2Sr_2Al_2O_7$ also present. This powder was made into slurry by dispersing it in methyl ethyl ketone along with organic additives as binder, surfactant, deflocculant and plasticizer followed by ball milling. BSAS glass powder, custom melted by an outside vendor, was also used as precursor to celsian matrix in the fabrication of some composite panels.

Schematic of the set-up used for fabrication of FRC by matrix slurry infiltration is shown in figure 4 (ref. 26). The fiber tows are impregnated with the matrix precursor by passing it through the slurry. Excess slurry is squeezed out of the fiber tow before winding it on a rotating drum. After drying, the prepreg tape is cut to size, stacked up in desired orientation, and warm pressed resulting in a "green" composite. The fugitive organics are slowly burned out of the sample in air followed by hot pressing in a graphite die resulting in almost fully dense composite.

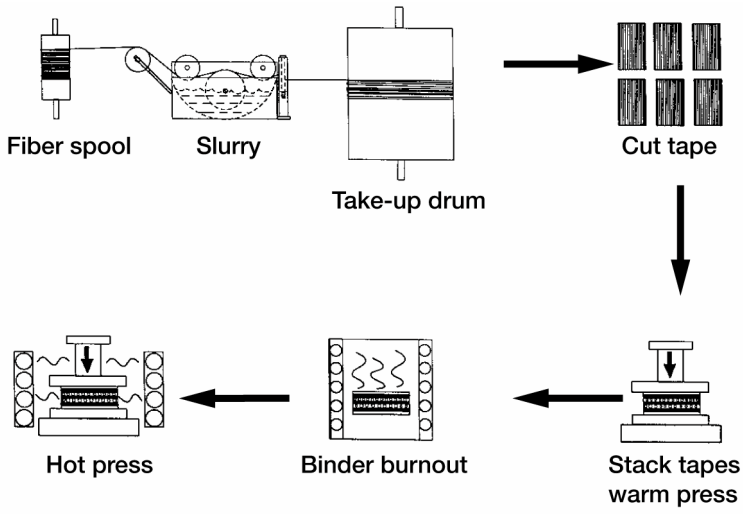

Figure 4.—Schematic of the set up used for fabrication of small diameter, multifilament fiber tow reinforced ceramic composites.

X-ray diffraction (fig. 5) from the surface of a hot pressed composite panel (ref. 27) showed only the desired monoclinic celsian. This indicates that the mixed oxide precursor is converted in situ into the monoclinic celsian phase during hot pressing of the FRC. The undesired hexacelsian phase was not detected from XRD. However, a small amount of hexacelsian was detected by Raman micro-spectroscopy (ref. 28). The hot pressed composite panel was surface polished and sliced into test bars for mechanical testing.

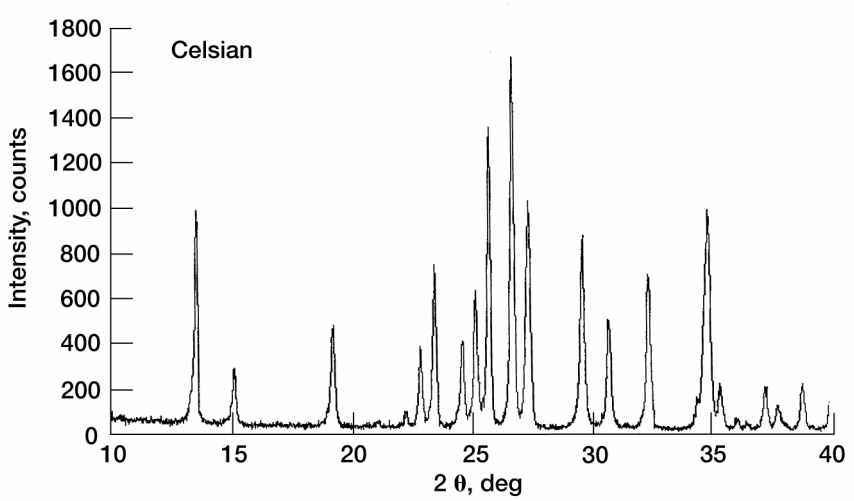

Figure 5.—X-ray diffraction from surface of a hot pressed Hi-Nicalon/BSAS composite.

Table 3.—Mechanical properties* of 0/90º Nicalon/BN/SiC/BSAS composites at various temperatures in air, V_f = 0.38 to 0.40

Temperature, ºC	Yield stress, σ_y MPa	Modulus, E_c GPa	Ultimate strength, σ_u MPa	Failure strain, percent
25	75 ± 1	92 ± 1	289 ± 9	0.43 ± 0.01
550	85 ± 1	88 ± 5	282 ± 21	0.45 ± 0.04
1100	60 ± 15	80 ± 6	208 ± 1	0.34 ± 0.01
1200	44 ± 5	63 ± 3	187 ± 20	0.39 ± 0.03
1300	32 ± 8	54 ± 3	180 ± 45	0.55 ± 0.10

*Measured in 4-point flexure

5. Nicalon/Celsian Composites

5.1 Flexure Strength

Flexure strength was measured in four-point bending using an upper span of 0.75 in. and a lower span of 2.5 in. Flexural properties (refs. 29 to 31) of 0/90° cross-ply Nicalon/BN/SiC/BSAS composites, containing 38 to 40 volume percent of fibers, at various temperatures in air are shown in table 3.

5.2 Effects of High-Temperature Annealing in Air

Thermal-oxidative stability of Nicalon/BN/SiC/BSAS composites has also been investigated (refs. 29 to 31). The 0/90° cross-ply composites, containing ~40 volume percent of fibers were heat treated in air for 100 to 500 hr. at various temperatures between ~550 °C to ~1300 °C. Glass formation was observed on the surface of specimens annealed at or above 1100 °C. The specimens exposed at ~1200 °C and ~1300 °C were so severely covered with glass, along with the presence of some gas bubbles, that these could not be further tested. The residual flexural strengths of the composites after air-annealing are shown

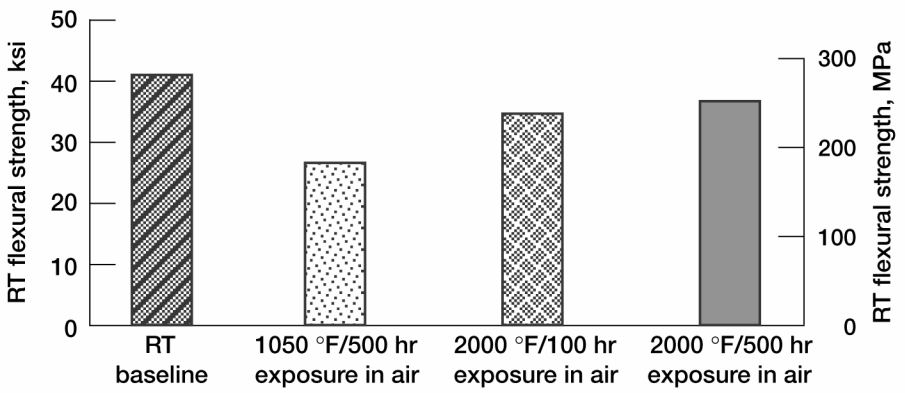

Figure 6.—Effect of air-annealing at various temperatures on room temperature flexural strength of (0/90) Nicalon/BSAS composites; V_f = 0.4.

in figure 6. The sample annealed at ~550 °C showed 40 percent drop in room temperature strength. This could be due to oxidation of the carbon layer (formed in situ during composite processing) at the fiber-matrix interface where the temperature is too low for any residual glassy phase to flow and provide oxidation resistance. However, the specimen exposed at ~1100 °C retained 90 percent of the baseline strength. At this temperature, the residual glassy phase is less viscous, as seen by gas bubble formation, and may have resulted in the protection of the carbon interface layer from oxidation.

5.3 Tensile Strength

Tensile testing was carried out in air at a displacement rate of 0.02 in./minute. Tensile properties of 0/90° cross-ply Nicalon/BN/SiC/BSAS composites, containing 38 to 40 volume percent of fibers, at various temperatures are shown (refs. 29 to 31) in table 4. Above ~1100 °C, ultimate strength and the proportional limit fall off fairly rapidly, while modulus decreased by ~40 percent from ambient temperature to ~1300 °C. Nicalon fiber is known to degrade at ~1200 °C and degradation rate increases with increase in temperature. Presence of residual glassy phase in the matrix would account for the observed decrease in modulus and increase in failure strain at elevated test temperatures.

Effect of test rate on ultimate tensile strength for 0/90° Nicalon/BSAS composite at 1100 °C in air has also been investigated (ref. 32). Results in figure 7 exhibit a significant dependency of ultimate strength on test rate. The ultimate strength decreased with decreasing test rate, similar to the behavior observed in many advanced monolithic ceramics (or brittle materials including glass and glass ceramics) at ambient or elevated temperature. The strength degradation with decreasing stress rate in brittle materials is known to occur by slow crack growth (delayed failure or fatigue) of an initial crack, and is expressed as:

$$\log \sigma_f = \frac{1}{n+1} \log \dot{\sigma} + \log D \tag{1}$$

where n and D are slow crack growth (SCG) parameters, and σ_f (MPa) and $\dot{\sigma}$ (MPa/s) are strength and stress rate, respectively. These results suggest that care must be exercised when characterizing elevated-temperature ultimate strength of composite materials. This is due to that fact that high-temperature ultimate strength has a relative meaning if a material exhibits rate dependency: the strength simply depends on which test rate one chooses. Therefore, at least two test rates (high and low) are recommended to better characterize the high-temperature ultimate strength behavior of a composite material.

Table 4.—Tensile properties of 0/90º Nicalon/BN/SiC/BSAS composites at various temperatures in air, V_f = 0.38 to 0.40

Temperature, ºC	Yield stress, σ_y MPa	Modulus, E_c GPa	Ultimate strength, σ_u MPa	Failure strain, percent
25	75 ± 1	97 ± 12	178 ± 28	0.43 ± 0.09
550	63 ± 1	87	196	0.64
1100	63 ± 6	71 ± 9	162 ± 16	0.41 ± 0.06
1200	32 ± 9	63 ± 3	112 ± 12	0.50 ± 0.08
1300	29 ± 2	53 ± 3	153 ± 3	0.63 ± 0.06

Table 5.—Interlaminar shear properties of 0/90º Nicalon/BN/SiC/BSAS composites at various temperatures in air, V_f = 0.38 to 0.40

Temperature, ºC	Interlaminar shear stress,* MPa	Failure mode
25	17 ± 2	Shear
1100	10 ± 3	Shear
1200	7 ± 1	Shear
1300	6 ± 1	Shear

*Average of three samples

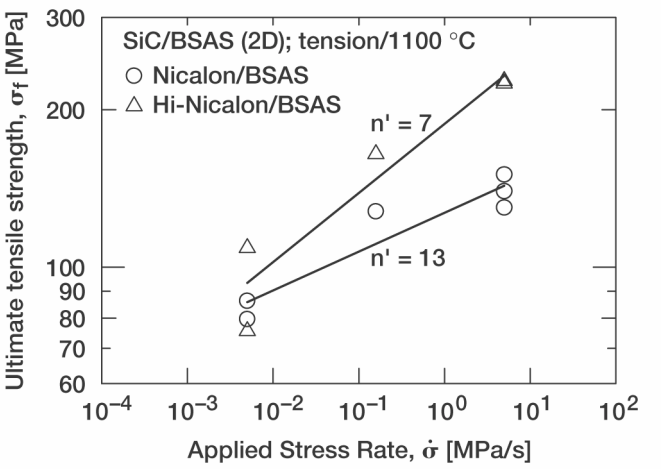

Figure 7.—Results of ultimate tensile strength as a function of applied stress rate determined for Nicalon/BSAS and Hi-Nicalon/BSAS composites at 1100 °C in air. The solid lines represent the best-fit regression based on eq. (1).

5.4 Shear Strength

Interlaminar shear testing was carried out using the short beam shear technique in 3-point bending at a displacement rate of 0.02 in./minute from room temperature to ~1300 ºC. Results of the interlaminar shear strength (ref. 31) for the 0/90° cross-ply Nicalon/BN/SiC/BSAS composites, containing 38 to 40 volume percent of fibers are given in table 5. The failure mode for all the test specimens was shear.

5.5 Tensile Stress-Rupture Strength

To determine if the composite would provide stress oxidative stability after the matrix is microcracked, stepped stress-rupture tests were carried out. The 0/90º cross-ply Nicalon/BN/SiC/BSAS composites, containing ~40 volume percent of fibers, were tested in standard dead weight creep machines at 1100 and 1200 ºC in air. No testing was done at 1300 ºC because of the presence of residual glass in the matrix. Tests were started at stress level near the proportional limit. Approximately every 50 hours, the stress was increased by 2 ksi (~14 MPa) until the sample failed. The results (ref. 31) are shown in figure 8. The composite survived to a stress level of ~60 percent of its ultimate tensile strength. Examination of the fracture surface of the specimen tested at ~1100 ºC/10 ksi (~70 MPa) for 8 hr. revealed some embrittlement.

Results of constant stress (stress-rupture) testing for 0/90º Nicalon/BSAS (for two different batches 'A' and 'B') at 1100 ºC in air are presented (ref. 32) in figure 9, where *time to failure* is plotted against *applied stress* in log-log scales. A decrease in time to failure with increasing applied stress, which represents a susceptibility to damage accumulation or delayed failure, is evident for the composite. The mode of fracture in constant stress testing was similar to that in constant stress-rate testing showing some fiber pullout with jagged matrix cracking through the specimen-thickness direction.

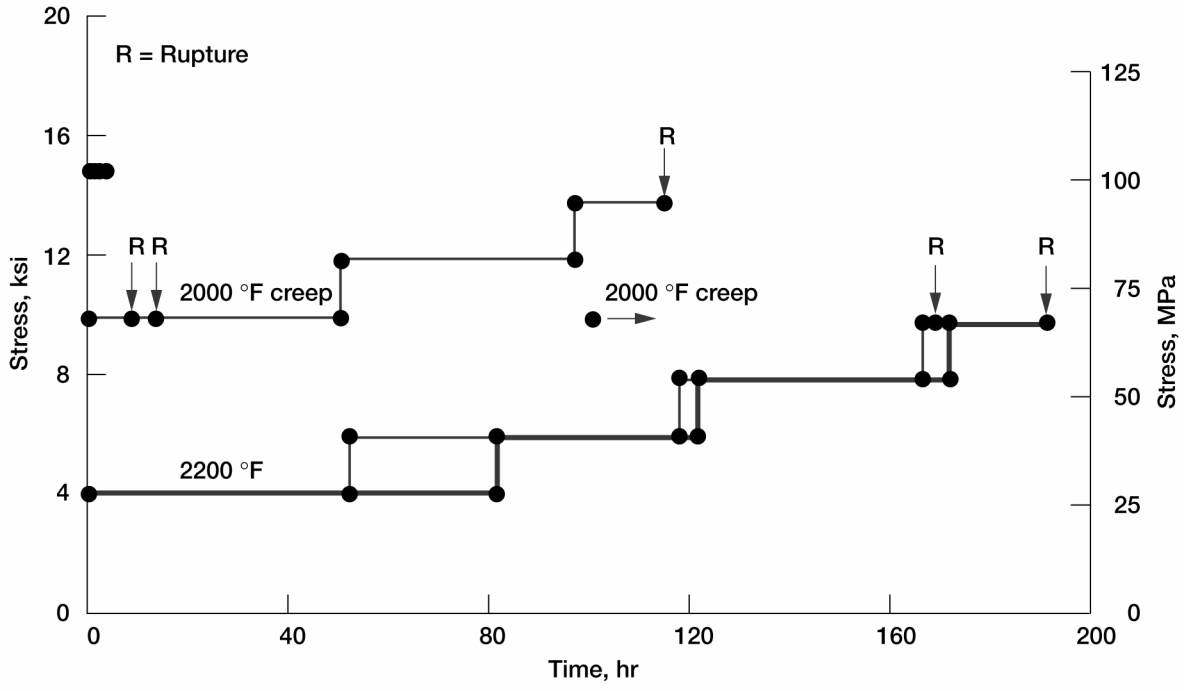

Figure 8.—Tensile stress rupture testing in air of (0/90) Nicalon/BSAS composites; $V_f = 0.4$

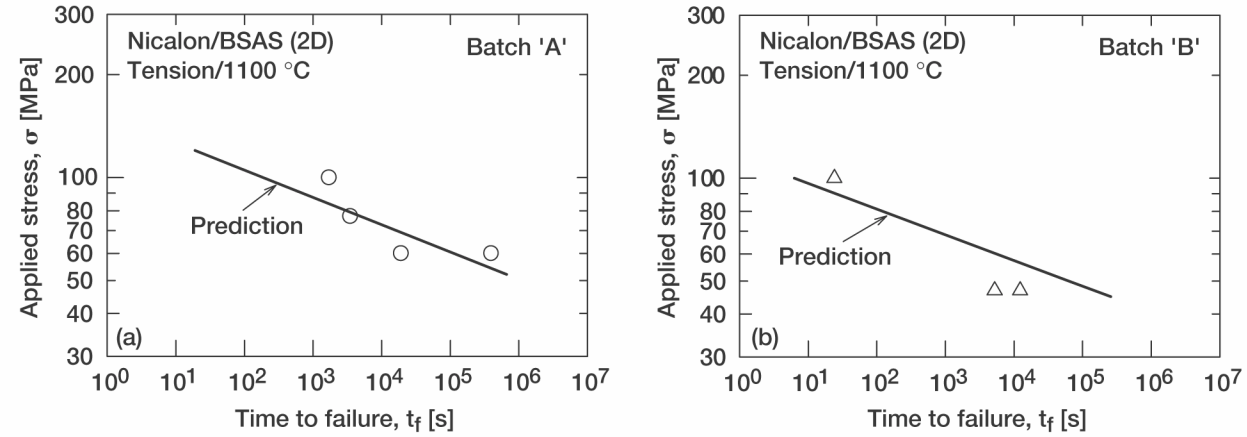

Figure 9.—Results of constant stress ("static fatigue" or "stress rupture") testing for Nicalon/BSAS composite: (a) Batch 'A' and (b) Batch 'B' tested at 1100 °C in air. The solid lines represent the predictions based on the results of constant stress-rate testing (Fig. 7).

6. Hi-Nicalon/Celsian Composites

SEM micrographs taken from the polished cross-sections of the uncoated and BN/SiC coated Hi-Nicalon fiber-reinforced BSAS composites are shown in figure 10. A large variation in fiber diameter within a tow can be seen although the manufacturer reports an average diameter of 14 μm. Uniform fiber distribution, good matrix infiltration within the fiber tow, and high composite density is evident. Occasional pores and second matrix phase, appearing as the bright phase, can also be seen. The amount of this second phase must be small, as it was not detected by XRD. This phase has been tentatively identified (ref. 33) as "hyalophane" [$(Ba,Sr)AlSi_3O_8$] which is richer in Si and deficient in Al than celsian. The BN coating which is the dark layer is adherent to the fiber, but the SiC coating tends to debond at the BN/SiC interface probably during composite processing.

TEM micrograph from the Hi-Nicalon/BN/SiC/BSAS composite (ref. 26) is shown in figure 11(a). Four distinct layers are seen in the BN coating. The SiC coating was often found to be missing from the BN/matrix interface but was intact in this particular case. Another TEM micrograph (ref. 26) is shown in figure 11(b). The fiber/BN interface and the innermost layer of BN are unchanged. BN has coarsened from outside inwards during composite processing. From EDS, no obvious chemical changes were observed in the BN coating. SiC layer was not affected.

6.1 Flexure Strength

Typical stress-strain curves, recorded in 3-point flexure, for the uncoated and BN/SiC coated fiber-reinforced composites (refs. 33 to 34) are shown in figure 12. Also shown for comparison is the stress-strain curve for a hot pressed BSAS monolith. The monolith shows bend strength of 130 MPa, modulus of 98 GPa and fails in brittle mode, as expected. The uncoated fiber-reinforced CMC shows a monolithic-like failure with strength of ~200 MPa and failure strain of ~0.1 percent. This shows that reinforcement of BSAS matrix with uncoated Hi-Nicalon fibers does not yield a strong or tough material. This may indicate a strong bond between the uncoated fibers and the matrix. However, fiber push-in and push-out tests (refs. 33 and 35) indicated a weak fiber-matrix interface in these CMCs. Low strength of these CMCs was found to be due to mechanical damage (refs. 33 and 35) to the fiber surface during hot pressing as no compliant layer (such as BN) was present. In contrast, the BN/SiC coated fiber-reinforced CMC shows graceful failure. The first matrix cracking stress was ~400 MPa and ultimate strength greater than 800 MPa. This shows that reinforcement of BSAS matrix with BN/SiC coated Hi-Nicalon fiber results in a strong and tough composite.

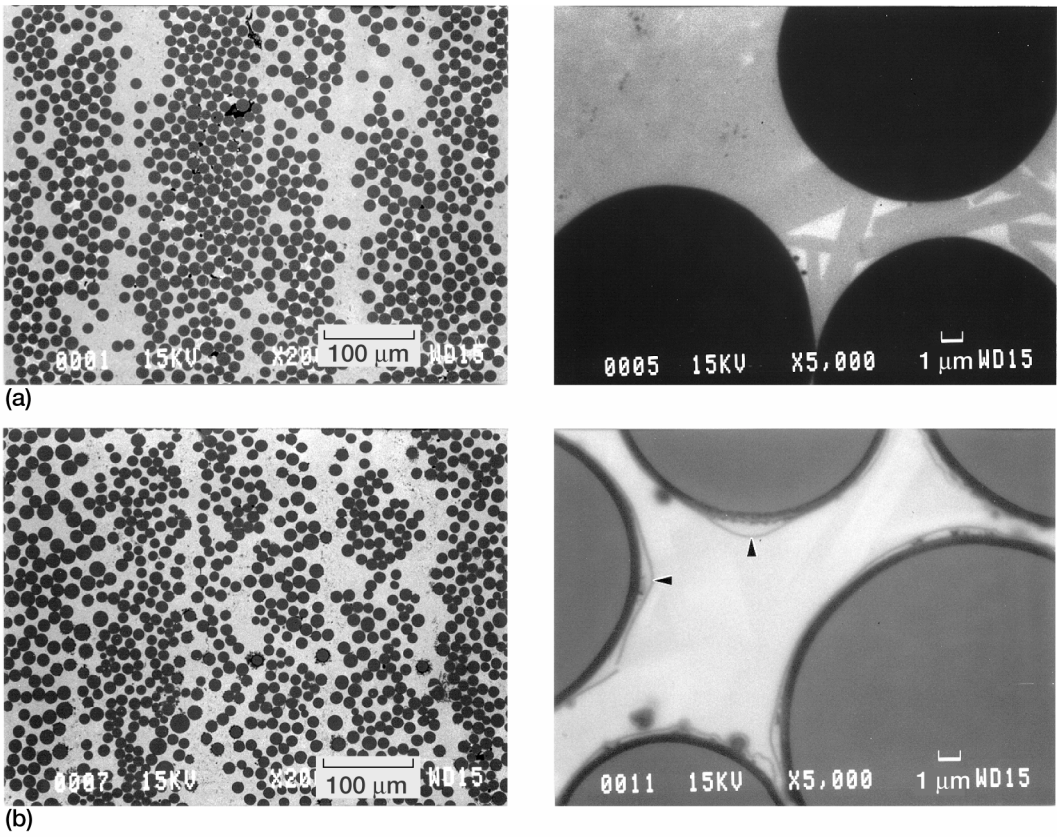

Figure 10.—SEM micrographs showing polished cross-sections of unidirectional (a) Hi-Nicalon (uncoated)/BSAS and (b) Hi-Nicalon/BN/SiC/BSAS composites.

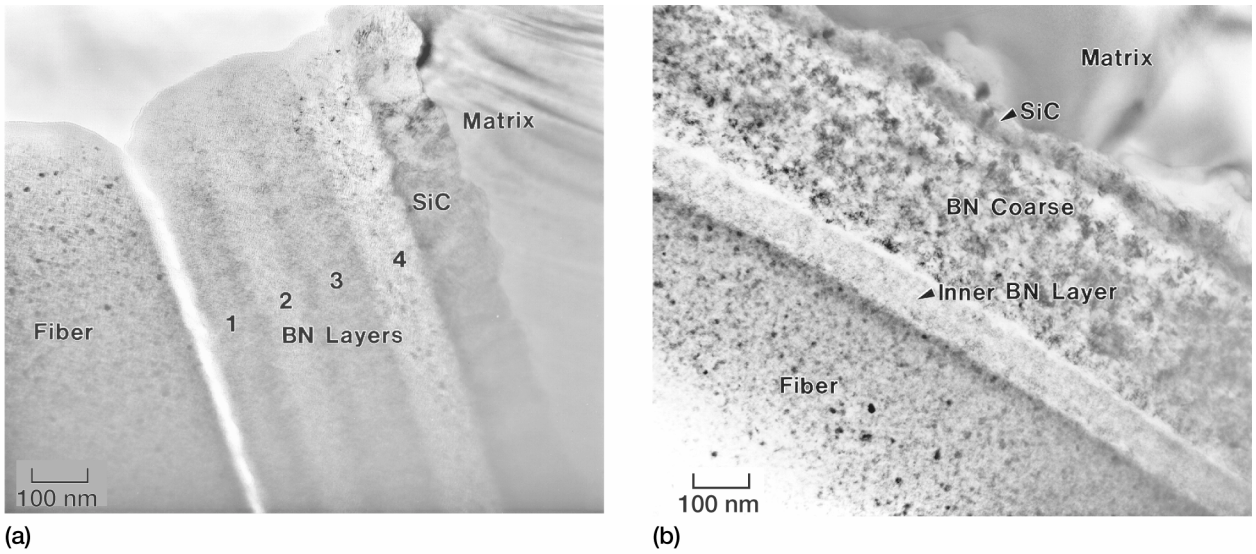

Figure 11.—TEM bright field image from cross-section of Hi-Nicalon/BN/SiC/BSAS composite showing (a) multiple BN layers and (b) coarsening of the outer three BN layers. The inner BN and the SiC interface layers are unaffected.

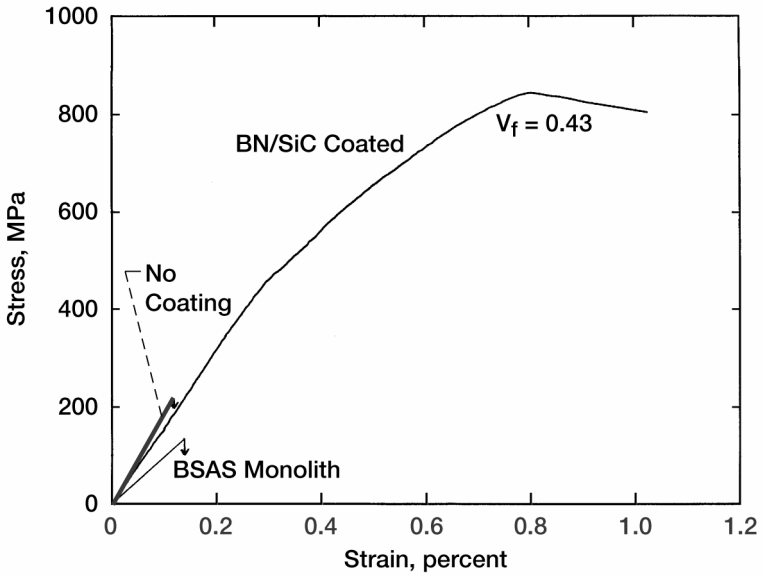

Figure 12.—Stress-strain curves for unidirectional uncoated and BN/SiC-coated Hi-Nicalon/BSAS composites recorded in 3-point flexure; also shown is the curve for hot pressed monolithic BSAS.

Table 6.—Tensile properties of unidirectional Hi-Nicalon/BN/SiC/BSAS composites at various temperatures in air, $V_f = 0.30$

Temperature, ºC	Modulus, E_c GPa	Yield stress, σ_y MPa	Yield strain, percent	Ultimate strength, σ_u MPa	Failure strain, percent
25	154 ± 2	97 ± 15	0.064 ± 0.09	589 ± 15	0.45 ± 0.01
800	132 ± 3	68 ± 6	0.052 ± 0.06	448 ± 4	0.41 ± 0.03
1000	106 ± 3	70 ± 7	0.064 ± 0.0 9	480 ± 25	0.40
1100	91 ± 3	92 ± 6	0.10 ± 0.005	400 ± 2	0.47 ± 0.05
1200	73 ± 5	99 ± 40	0.074	370 ± 12	--

6.2 Tensile Strength

Tensile properties of unidirectional BN/SiC coated Hi-Nicalon fiber reinforced celsian matrix composites (refs. 36 and 37) from room temperature to 1200 ºC in air are shown in table 6. The value of Young's modulus decreased with increase in test temperature indicating the presence of glassy phase in the matrix. The yield stress decreased from room temperature to 800 ºC followed by a slight increase to 1200 ºC. Ultimate strength decreased with temperature. SEM micrographs of the fracture surfaces of the composite specimens after tensile tests showed extensive fiber pullout. Fracture surfaces of samples tested at 1000 ºC or higher showed the presence of pores in the matrix which were more predominant in the 1200 ºC tested specimen. This may be due to oxidation of the Hi-Nicalon fibers producing a gaseous product and also oxidation of the BN coating producing a low melting glassy phase that is partially blown out of the interior of the composite by the escaping gases.

Effect of test rate on ultimate tensile strength of 0/90º Hi-Nicalon/BSAS composite at 1100 ºC in air has also been investigated (ref. 32). Results in figure 7 exhibit a significant dependency of ultimate strength on test rate. The ultimate strength decreased with decreasing test rate, similar to the behavior observed in many advanced monolithic ceramics (or brittle materials including glass and glass ceramics) at ambient or elevated temperature.

6.3 Shear Strength

In-plane and interlaminar shear strength of composites have been measured by the double-notch shear test method at a displacement rate of 2×10^{-3} mm/s. Results for a unidirectional Hi-Nicalon/BN/SiC/BSAS composite containing 42 volume percent of fibers from room temperature to 1200 ºC are shown (refs. 38 and 39) in figure 13. The interlaminar shear strength is lower than the in-plane shear strength at all temperatures. A rapid decrease in strength with temperature is probably due to softening of the residual glassy phase in the matrix.

Test rate dependence of interlaminar and in-plane shear strengths of CMC have also been investigated (refs. 40 and 41) using double notch shear (DNS) test specimens. Typical load versus time curves for two different test rates are shown in figure 14. The effects of test rate on shear strengths of a unidirectional Hi-Nicalon™ fiber-reinforced BSAS composite at 1100 ºC in air are presented in figure 15. The composite exhibited a significant effect of test rate on shear strength, regardless of orientation which was either in interlaminar or in in-plane region. Shear-strength degraded by about 50 percent as test rate decreased from 3.3×10^{-1} mm/s to 3.3×10^{-5} mm/s. The rate dependency of composite's shear strength was very similar to that of ultimate tensile strength at 1100 ºC observed (ref. 32) in a similar composite (2-D Hi-Nicalon/BSAS) in which ultimate tensile strength decreased by about 60 percent when test rate changed from the highest (5 MPa/s) to the lowest (0.005 MPa/s). A phenomenological, power-law slow crack growth formulation has been proposed (refs. 40 and 41) to account for the rate dependency of shear strength of the composite.

Results of shear strength (τ_f) as a function of applied shear stress rate ($\dot{\tau}$) based on

$$\log\tau_f = \frac{1}{n_s+1}\log\dot{\tau} + \log D_s \tag{2}$$

with displacement rate being converted to shear stress rate are shown in figure 16. Here n_s and D_s are the slow crack growth (SCG) parameters. The values of SCG parameters were determined as n_s = 11.2 and D_s = 19.24 for interlaminar direction and n_s = 11.4 and D_s = 33.27 for in-plane direction. It is noteworthy that the value of n_s, a measure of susceptibility to SCG, was same in both directions. The value of SCG parameter n_s (= 11) in shear also compares with that of n (= 7) in tension for the similar 2-D Hi-Nicalon/BSAS composite tested at 1100 ºC in air (ref. 32), indicating that the Hi-Nicalon/BSAS composites exhibit significant susceptibility to SCG in both shear and tension. In general, the patterns of SCG for many monolithic advanced ceramics tested at elevated temperatures are well defined in fracture surfaces in terms of its configuration and size. By contrast, the patterns of SCG for CMCs subjected to either in tension or in shear are not obvious and rather obscured by the nature of composite architecture so that it would be very difficult and/or a great challenge to derive a definite evidence of SCG from overall fracture surface examinations. Hence, the study of shear strength degradation with respect to test rate through constant stress-rate testing is a simple, quick and convenient way to check and quantify the degree of SCG in shear for CMCs at elevated temperatures. The residual glassy phase may have been a major cause of SCG in the Hi-Nicalon/BSAS composite under shear. Life prediction diagram (applied shear stress vs. time to failure) in shear for interlaminar and in-plane directions for Hi-Nicalon/BSAS composite (ref. 41) at 1100 ºC in air is shown in figure 17.

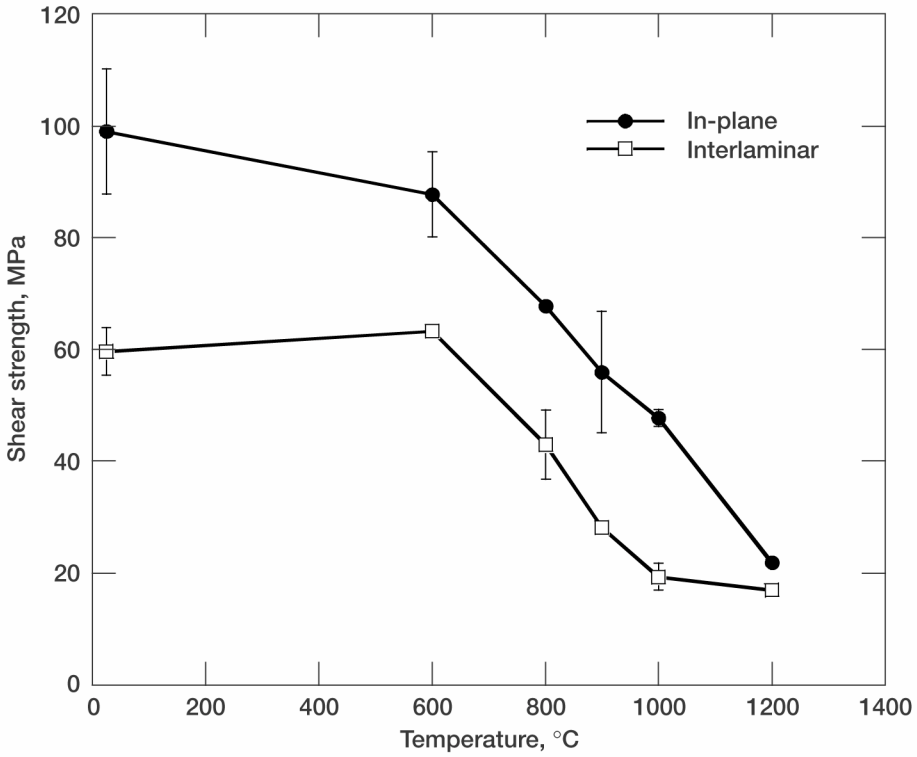

Figure 13.—Temperature dependence of interlaminar and in-plane shear strength of Hi-Nicalon/BSAS composite in air.

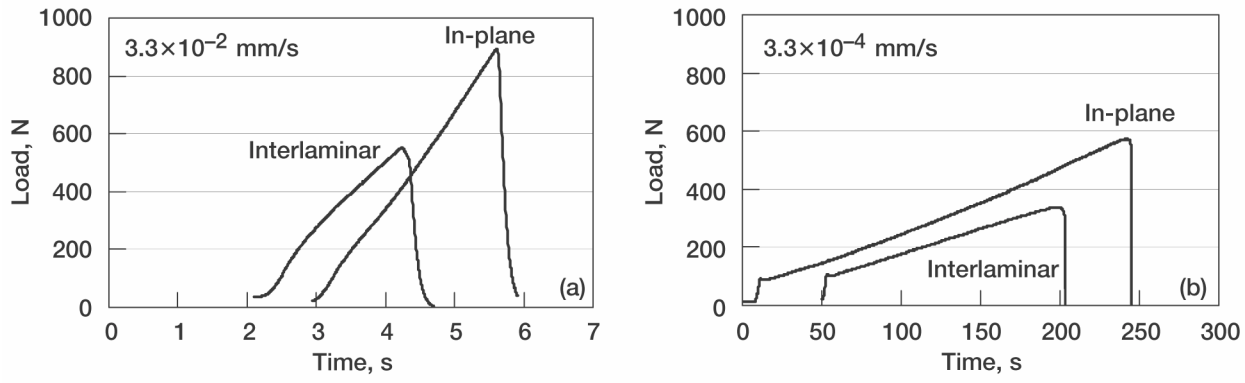

Figure 14.—Typical load-time curves for Hi-Nicalon/BSAS composite tested in interlaminar and in-plane shear at 1100 °C in air. (a) Fast test rate of 3.3×10^{-2} mm/s. (b) Slow test rate of 3.3×10^{-4} mm/s.

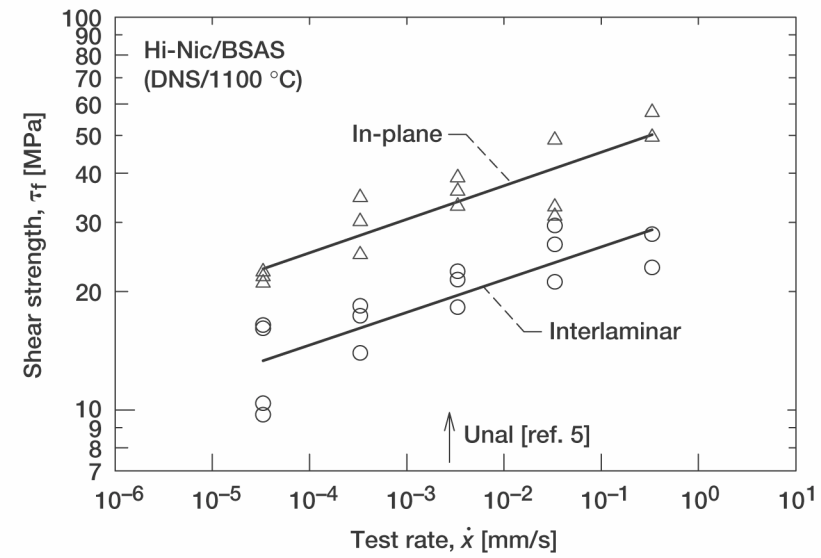

Figure 15.—Effect of test rate on interlaminar and in-plane shear strengths for Hi-Nicalon/BSAS composite tested at 1100 °C in air. The arrow in the 'test-rate' axis indicates the test rate used by Unal and Bansal [38-39].

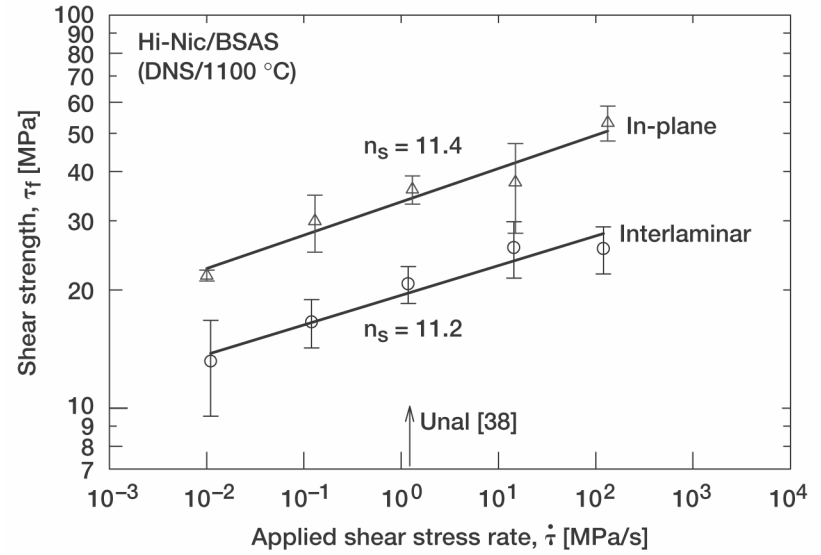

Figure 16.—Shear strength as a function of applied shear stress rate for Hi-Nicalon/BSAS composite at 1100 °C in air, reconstructed from the data in Fig. 15 based on eq. (2). The arrow in the 'stress-rate' axis indicates the stress rate used by Unal and Bansal [38-39].

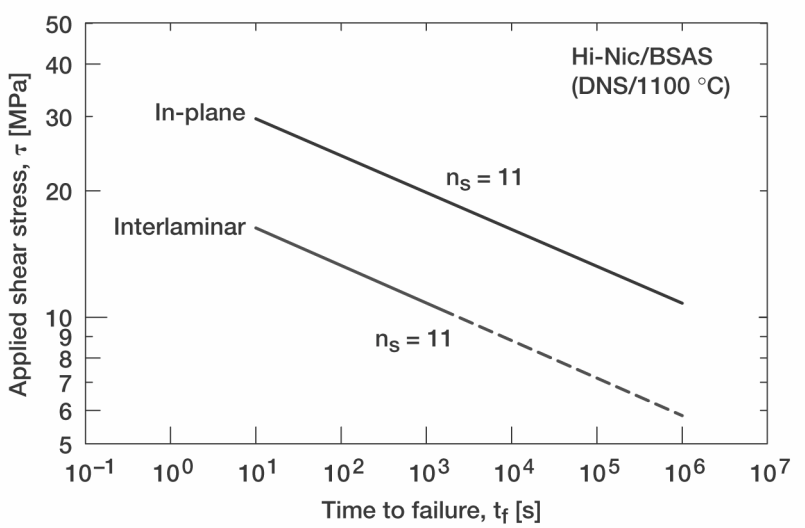

Figure 17.—Life prediction diagram in shear for Hi-Nicalon/BSAS composite at 1100 °C in air in-interlaminar and in-inplane directions under constant stress condition.

6.4 Thermo-Oxidative Stability

6.4.1 Effects of high-temperature annealing in air.—Thermal-oxidative stability of Hi-Nicalon/BN/SiC/BSAS composites has also been investigated (refs. 42 and 43). Unidirectional composites were annealed for 100 hr. in air at various temperatures. Optical photographs showing the physical appearance of the CMC bars before and after annealing at various temperatures are shown in figure 18. No changes in physical appearance were observed in samples annealed at 1000 ºC or lower. However, the specimen annealed at 1100 ºC was covered with a thin porous white layer that could be easily removed by polishing with a fine emery paper. The samples aged at 1200 ºC were deformed and developed a thick shiny white glaze on the exposed surfaces. Pores were present in the surface layer. Signs of partial melting and gas bubble formation during heat treatment were also observed. From XRD analysis, both amorphous and Celsian phases were detected in the surface layer. Since such a behavior was not observed (ref. 44) in monolithic BSAS material even after heat treatment for 20 hr. in air at 1500 ºC, it must be caused by the presence of Hi-Nicalon fibers and/or the BN/SiC coating. In air, BN is probably oxidized to B_2O_3 which reacts with the matrix and/or silica formed from the oxidation of silicon carbide fibers, resulting in low-melting glassy phase which migrates to the sample surface. The bubble formation may be related to the oxidation of Hi-Nicalon fibers producing amorphous silica and CO and CO_2 gases.

The matrix layers on the surface of CMC specimens annealed at 1100 and 1200 ºC appear to have cracked and delaminated as seen in the SEM micrographs (fig. 19), taken from the polished cross-sections. A large difference in the coefficients of thermal expansion (CTE) of Hi-Nicalon fiber ($\sim 3.5\times10^{-6}$/ºC) and the matrix may be responsible for the observed cracking and delamination. This would provide an easy path for the ingression of oxygen to the fiber bundles and accelerate the degradation of fibers from oxidation. No such cracking or delamination was observed in samples annealed at lower temperatures. Higher magnification SEM micrographs from the 1200 ºC annealed specimens showed the presence of gas bubbles on its surface. Severe damage was also observed underneath the top debonded layer where damaged broken pieces of the fibers are also present.

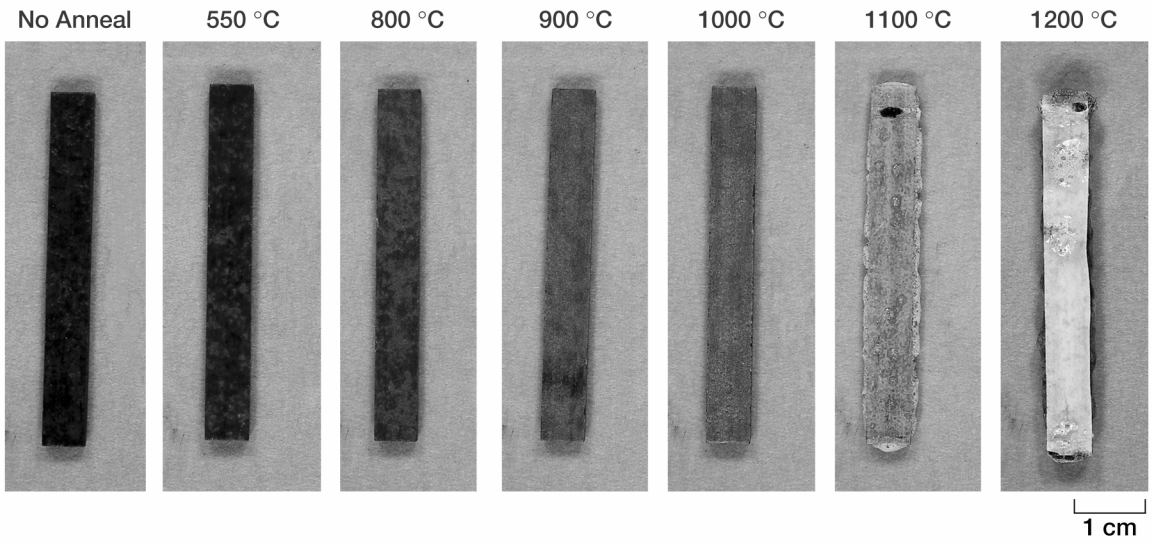

Figure 18.—Optical photographs showing surface appearance of Hi-Nicalon/BSAS composites after 100 h air-annealing at various temperatures.

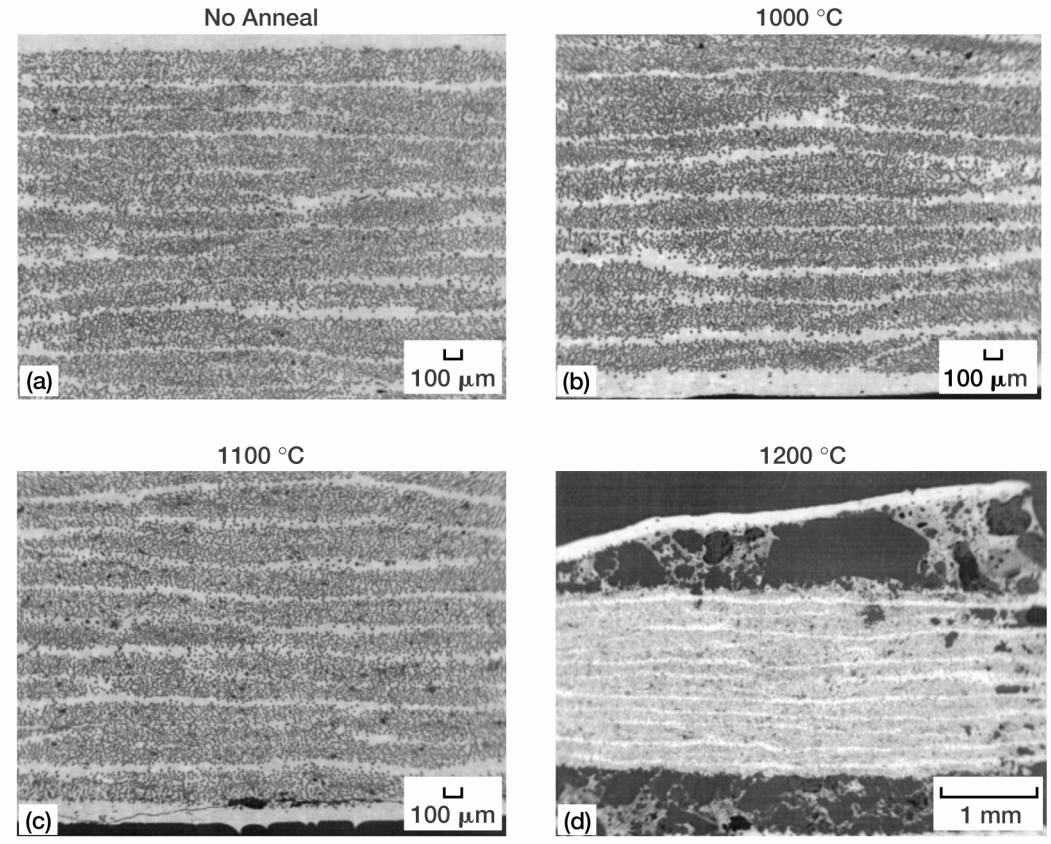

Figure 19.—SEM micrographs showing polished cross-sections of unidirectional Hi-Nicalon/BSAS composites annealed for 100 h in air at various temperatures; V_f = 0.32.

Table 7. Mechanical properties* of unidirectional Hi-Nicalon/BN/SiC/BSAS composites annealed at various temperatures for 100 hr. in air, $V_f = 0.32$

Annealing Temperature, ºC	Density, g/cm^3	Weight change after annealing, percent	E_c, GPa	σ_y, MPa	ε_y, percent	σ_u, MPa
------	3.09 ± 0.03	--	137	122	0.091	759
550	3.12	--	145	155	0.108	853
800	3.06	--	150	138	0.096	814
900	3.16	--	151	171	0.114	769
1000	3.04	--	146	134	0.092	819
1100	2.90	--	142	143	0.102	736
1200	Deformed	+0.43	--	--	--	--

*Measured at room temperature in 3-point flexure

Flexure strengths of the annealed CMC specimens were measured at room temperature in 3-point bending. The strain-stress curves of the CMCs annealed at various temperatures are presented in figure 20 and the results are summarized in table 7. Up to the annealing temperature of 1100 ºC, no net change was observed in the weights of samples. Also, values of Young's modulus (E_c), yield stress (σ_y), yield strain (ε_y), and ultimate strength (σ_u) did not change. However, the specimen annealed at 1200 °C, gained 0.43 percent weight and had appreciably deformed and its strength could not be measured.

6.4.2 Degradation mechanism at 1200 °C.—Various steps involved in the degradation of Hi-Nicalon/BN/ SiC/BSAS CMC on annealing in air at 1200 ºC are shown in figure 21. During annealing at 1200 ºC, the surface matrix layer delaminates from the composite ply underneath (SEM micrograph of fig. 19), probably due to the large CTE mismatch between the Hi-Nicalon fibers and the celsian matrix. This facilitates the ingression of oxygen into the composite. This causes the oxidation of SiC fibers, particularly those which have lost the duplex CVD coating (see fig. 10), resulting in the formation of SiO_2:

$$SiC\,(s) + O_2\,(g) \rightarrow SiO_2\,(s) + CO\,(g) + CO_2\,(g) \qquad (3)$$

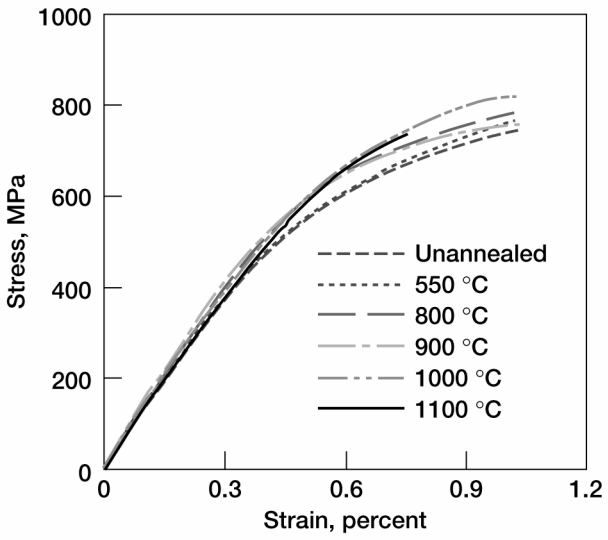

Figure 20.—Room temperature stress-strain curves recorded in 3-point flexure for unidirectional Hi-Nicalon/BSAS composites annealed for 100 h in air at various temperatures; $V_f = 0.32$.

The silica formed reacts with celsian resulting in the formation of a low melting phase. The phase diagram of $BaO\text{-}Al_2O_3\text{-}SiO_2$ system (fig. 22) (ref. 45) does show the presence of a ternary phase with a melting point of 1122 ºC. This phase is richer in SiO_2 but poorer in BaO and Al_2O_3 than celsian. Formation of gaseous by-products CO and CO_2 during reaction (3) results in the evolution of bubbles as observed in SEM micrograph of figure 19. On cooling, celsian crystals precipitate from the melt leaving behind a glassy matrix which is richer in SiO_2 and poorer in BaO and Al_2O_3 than celsian. SEM micrograph taken from the surface of CMC annealed at 1200 ºC showed the presence of elongated crystals in glassy matrix. From qualitative EDS analysis, these crystals were seen to be celsian and the glassy matrix was richer in SiO_2 but poorer in BaO and Al_2O_3 than celsian. The XRD analysis showed only celsian in the as-fabricated sample whereas celsian and an amorphous phase were present in the 1200 ºC-annealed CMC. Formation of a low-melting glass

phase has also been reported (ref. 3) in the study of BSAS environmental barrier coating (EBC) on Si-based ceramic substrates such as CVD SiC and SiC_f/SiC composite. On heat treatment, the plasma sprayed BSAS coating reacted with the silica layer, formed from oxidation of the Si-based ceramic substrate, resulting in low melting ternary glass phase which was found to be richer in SiO_2 but poorer in BaO and Al_2O_3 than celsian.

- Delamination of surface matrix layer in FRC
- Ingression of oxygen into FRC
- Oxidation of SiC fibers:

$$SiC + O_2 \rightarrow SiO_2 + CO + CO_2$$

- Reaction of SiO_2 and Celsian:

$$\text{Celsian} + SiO_2 \rightarrow \text{Low m.p. ternary phase}$$

- On cooling: formation of Celsian crystals in glass matrix

Figure 21.—Proposed degradation mechanism of Hi-Nicalon/BSAS composites at 1200 °C in air.

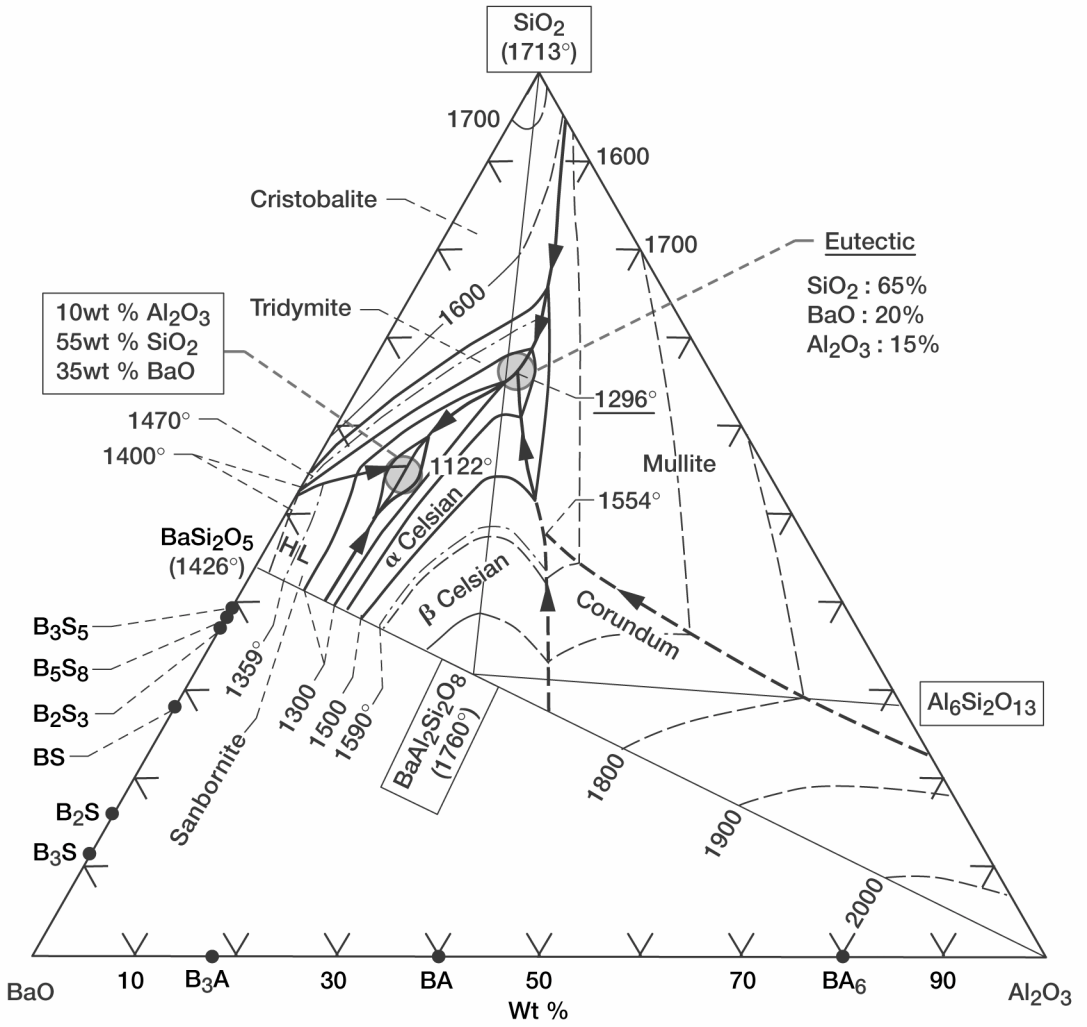

Figure 22.—Phase diagram of $BaO\text{-}Al_2O_3\text{-}SiO_2$ system.

7. Concluding Remarks

Hi-Nicalon/Celsian composites are stable up to use temperature of ~1100 ºC in oxidizing environments and degrade at higher temperatures due to the instability of polymer-derived fibers. The stability of Celsian matrix composites may be extended to higher temperatures by more uniform and stable interface coating(s) and by reinforcement with more advanced silicon carbide fiber (Sylramic) for applications as hot components (combustion liner, air foil, nozzle, etc.) in turbine engines.

References

1. Prewo, K.M., Fiber Reinforced Glasses and Glass-Ceramics, in "Glasses and Glass- Ceramics," Lewis, M.H., Ed., Chapman and Hall, New York, NY, 1989; pp. 336–368.
2. Brennan, J.J., Glass and Glass-Ceramic Matrix Composites, in "Fiber Reinforced Ceramic Composites. Materials, Processing and Technology," Mazdiyasni, K.S., Ed., Noyes Publications, Park Ridge, NJ, 1990, pp. 222–259.
3. Lee, K.N., Fox, D.S., Eldridge, J.I., Zhu, D., Robinson, R.C., Bansal, N.P., and Miller, R.A., Upper Temperature Limit of Environmental Barrier Coatings Based on Mullite and BSAS, NASA/TM—2002-211372, March 2002. *J. Am. Ceram. Soc*., **86** [8] 1299–1306 (2003).
4. Eaton, Jr., H.E., Allen, W.P., Jacobson, N.S., Bansal, N.P., Opila, E.J., Smialek, J.L., Lee, K.N., Spitsberg, I.T., Wang, H., Meschter, P.J., and Luthra, K.L., Silicon Based Substrate with Environmental/ Thermal Barrier Layer, U.S. Patent 6,387,456; May 14, 2002.
5. Bansal, N.P., Ceramic Fiber-Reinforced Glass-Ceramic Matrix Composites, U.S. Patent 5,214,004; May 25, 1993.
6. Bansal, N.P., Method of Producing a Ceramic Fiber-Reinforced Glass-Ceramic Matrix Composite, U.S. Patent 5,281,559; January 25, 1994.
7. Bansal, N.P., Method of Producing a Silicon Carbide Fiber Reinforced Strontium Aluminosilicate Glass-Ceramic Matrix Composite, U.S. Patent 5,389,321; February 14, 1995.
8. Bansal, N.P., Mechanical Behavior of Silicon Carbide Fiber-Reinforced Strontium Aluminosilicate Glass-Ceramic Composites, *Mater. Sci. Eng. A,* **231** [1–2] 117–127 (1997).
9. Bansal, N.P., CVD SiC (SCS-0) Fiber-Reinforced Strontium Aluminosilicate Glass-Ceramic Composites, *J. Mater. Res*., **12** [3] 745–753 (1997).
10. Bansal, N.P., Influence of Fiber Volume Fraction on Mechanical Behavior of CVD SiC Fiber/$SrAl_2Si_2O_8$ Glass-Ceramic Matrix Composites, *SAMPE J. Advanced Mater*., **28** [1] 48–58 (1996).
11. Bansal, N.P., CVD SiC Fiber-Reinforced Barium Aluminosilicate Glass-Ceramic Matrix Composites, *Mater. Sci. Eng. A*, **220** [1–2] 129–139 (1996).
12. Bansal, N.P., Celsian Formation in Fiber-Reinforced Barium Aluminosilicate Glass-Ceramic Matrix Composites, *Mater. Sci. Eng*. A, **342** [1–2] 23–27 (2003).
13. Moya Corral, J.S., and Verduch, G., The Solid Solution of Silica in Celsian, *Trans. J. Br. Ceram. Soc*., **77**, 40–44 (1978).
14. Bahat, D., Kinetic Study on the Hexacelsian-Celsian Phase Transformation, *J. Mater. Sci*., **5,** 805–810 (1970).
15. Yoshiki, B., and Matsumoto, K., High Temperature Modification of Barium Feldspar*, J. Am. Ceram. Soc*., **34** [9], 283–286 (1951).
16. Takeuchi, Y., A Detailed Investigation of the Structure of Hexagonal $BaAl_2Si_2O_8$ With Reference to its α-beta Inversion, *Min. J. Japan*, **2**[5], 311–332 (1958).
17. Newnham, R.E., and Megaw, H.D., The Crystal Structure of Celsian (Barium Feldspar), *Acta Cryst*., **13**, 303–312 (1960).
18. Gay, P., A Note on Celsian, *Acta Cryst*., **9**, 474 (1956).

19. Guillem, M.C., and Guillem, C., Kinetics and Mechanism of Formation of Celsian from Barium Carbonate and Kaolin, *Trans. J. Br. Ceram. Soc*., **83**, 150–154 (1984).
20. Bansal, N.P., Solid State Synthesis and Properties of Monoclinic Celsian, *J. Mater. Sci*., **33** [19] 4711–4715 (1998).
21. Buzniak, J.J., Lagerlof, K.P.D., and Bansal, N.P., Hot Pressing and High Temperature Mechanical Properties of $BaAl_2Si_2O_8$ (BAS) and $SrAl_2Si_2O_8$ (SAS), in Advances in Ceramic Matrix Composites (Bansal N.P., Ed.), Am. Ceram. Soc., Westerville, OH; *Ceram. Trans*., **38**, 789–801 (1993).
22. Zhu, D., Bansal, N.P., Lee, K.N., and Miller, R.A., Thermal Conductivity of Ceramic Thermal Barrier and Environmental Barrier Coating Materials, NASA/TM—2001-211122, Sept. 2001.
23. Bansal, N.P., and Hyatt, M.J., Crystallization Kinetics of Barium Aluminosilicate Glasses, *J. Mater. Res*., **4** 1257 (1989).
24. Hyatt, M.J., and Bansal, N.P., Crystal Growth Kinetics in $BaOAl_2O_32SiO_2$ and $SrOAl_2O_32SiO_2$ Glasses, *J. Mater. Sci*., **31**[1] 172–184 (1996).
25. Bansal, N.P., and Drummond III, C.H., Kinetics of Hexacelsian to Monoclinic Celsian Phase Transformation in $SrAl_2Si_2O_8$, *J. Am. Ceram. Soc*., **76** 1321 (1993).
26. Bansal, N.P., and Setlock, J.A., Fabrication of Fiber-Reinforced Celsian Matrix Composites, *Comp. Part A: Applied Science and Manufacturing*, **32**[8] 1021–1029 (2001).
27. Bansal, N.P., Strong and Tough Hi-Nicalon Fiber-Reinforced Celsian Matrix Composites, *J. Am. Ceram. Soc*., **80** [9] 2407–2409 (1997).
28. Gouadec, G., Colomban, P., and Bansal, N.P., Raman Study of Hi-Nicalon Fiber-Reinforced Celsian Composites. Part 1: Distribution and Nanostructure of Different Phases, *J. Am. Ceram. Soc*., **84**[5] 1129–1135 (2001).
29. Bansal, N.P., McCluskey, P.H., Linsey, G.D., Murphy, D., and Levan, G., Processing and Properties of Nicalon Reinforced Barium Aluminosilicate (BAS) Glass-Ceramic Matrix Composites, in *Ceramic Matrix Composites for Rocket Nozzle, Leading Edge, and Turbine Applications*, Opeka, M.M., Ed., DoD Ceramics Information Analysis Center, West Lafayette, IN; pp. 335–358 (1995).
30. Bansal, N.P., McCluskey, P.H., Linsey, G.D., Murphy, D., and Levan, G., Nicalon Fiber-Reinforced Celsian Glass-Ceramic Composites, in "HITEMP Review 1995 - Advanced High Temperature Engine Materials Technology Program. *Volume III: Turbine Materials ---CMC's, Fiber and Interface Issues*," NASA CP–10178, pp. 41–1 to 41–14 (1995).
31. Linsey, G.D., McCluskey, P., Murphy, D., and Levan, G., Processing and Properties of Barium Aluminosilicate Glass-Ceramic Matrix Composites, NASA CR–198369, August 1995.
32. Choi, S.R., Bansal, N.P., and Gyekenyesi, J.P., Ultimate Tensile Strength as a Function of Test Rate for Various Ceramic Matrix Composites at Elevated Temperatures, NASA/TM—2002-211579, June 2002.
33. Bansal, N.P., and Eldridge, J.I., Hi-Nicalon Fiber-Reinforced Celsian Matrix Composites: Influence of Interface Modification, *J. Mater. Res*., **13** [6] 1530–1537 (1998).
34. Ünal, Ö., and Bansal, N.P., Temperature Dependency of Strength of a Unidirectional SiC Fiber-Reinforced $(Ba,Sr)Al_2Si_2O_8$ Celsian Composite, in *Advances in Ceramic Matrix Composites IV* (Singh, J.P., and Bansal, N.P., Eds.), Am. Ceram. Soc., Westerville, OH; *Ceram. Trans*., **96**, 135–147 (1999).
35. Bansal, N.P., and Eldridge, J.I., Effects of Fiber/Matrix Interface and its Composition on Mechanical Properties of Hi-Nicalon/Celsian Composites, NASA/TM—1999-209057, March 1999; *Proc. ICCM-12 Conference*, Paper No. 147, Paris, France, July 1999; ISBN 2–9514526–2–4.
36. Gyekenyesi, J.Z., and Bansal, N.P., High Temperature Mechanical Properties of Hi-Nicalon Fiber-Reinforced Celsian Composites, in *Advances in Ceramic Matrix Composites V* (Bansal, N.P., Singh, J.P., and Ustundag, E., Eds.), Am. Ceram. Soc., Westerville, OH; *Ceram. Trans*., **103**, 291–306 (2000).
37. Gyekenyesi, J.Z., and Bansal, N.P., High Temperature Tensile Properties of Unidirectional Hi-Nicalon/ Celsian Composites in Air, NASA/TM—2000-210214, July 2000.
38. Ünal, Ö., and Bansal, N.P., Interlaminar Shear Strength of a Unidirectional Fiber-Reinforced Celsian Composite by Short-Beam and Double-Notched Shear Tests, *Ceram. Eng. Sci. Proc*., **22** [3] 585–595 (2001).

39. Ünal, Ö., and Bansal, N.P., In-Plane and Interlaminar Shear Strength of Silicon Carbide Fiber-Reinforced Celsian Composite, *Ceram. Int*., **28** [5] 527–540 (2002).
40. Choi, S.R., Bansal, N.P., and Gyekenyesi, J.P., Rate Dependency of Shear Strength in SiC_f/BSAS Composite at Elevated Temperature, *Ceram. Eng. Sci. Proc*., **24** (2003).
41. Choi, S.R., Bansal, N.P., and Gyekenyesi, J.P., Dependency of Shear Strength on Test Rate in SiC/BSAS Ceramic matrix Composite at Elevated Temperature, NASA/TM—2003-212182, April 2003.
42. Bansal, N.P., Mechanical Properties of SiC Fiber-Reinforced Celsian Composites After High-Temperature Exposures in Air, in *Proc. 8th International Conference on Composites Engineering (ICCE-8),* Hui, D., Ed., Tenerife, Spain, August 5–11 (2001); p. 59.
43. Bansal, N.P., Effects of Thermal Ageing in air on Microstructure and Mechanical Properties of Hi-Nicalon Fiber-Reinforced Celsian Composites, unpublished work.
44. Bansal, N.P., Hyatt, M.J., and Drummond III, C.H., Crystallization and Properties of Sr-Ba Aluminosilicate Glass-Ceramic Matrices, *Ceram. Eng. Sci. Proc*., **12** [7–8] 1222–1234 (1991).
45. Levin, E.M., and McMurdie, H.F., Phase Diagram for Ceramists, Vol. III, Fig. 4544, p. 220 (1975); The Am. Ceram. Soc., Westerville, OH.

REPORT DOCUMENTATION PAGE

Form Approved
OMB No. 0704-0188

Public reporting burden for this collection of information is estimated to average 1 hour per response, including the time for reviewing instructions, searching existing data sources, gathering and maintaining the data needed, and completing and reviewing the collection of information. Send comments regarding this burden estimate or any other aspect of this collection of information, including suggestions for reducing this burden, to Washington Headquarters Services, Directorate for Information Operations and Reports, 1215 Jefferson Davis Highway, Suite 1204, Arlington, VA 22202-4302, and to the Office of Management and Budget, Paperwork Reduction Project (0704-0188), Washington, DC 20503.

1. AGENCY USE ONLY (*Leave blank*)	2. REPORT DATE	3. REPORT TYPE AND DATES COVERED
	August 2003	Technical Memorandum

4. TITLE AND SUBTITLE

SiC Fiber-Reinforced Celsian Composites

5. FUNDING NUMBERS

WBS–22–708–31–11

6. AUTHOR(S)

Narottam P. Bansal

7. PERFORMING ORGANIZATION NAME(S) AND ADDRESS(ES)

National Aeronautics and Space Administration
John H. Glenn Research Center at Lewis Field
Cleveland, Ohio 44135–3191

8. PERFORMING ORGANIZATION REPORT NUMBER

E–14121

9. SPONSORING/MONITORING AGENCY NAME(S) AND ADDRESS(ES)

National Aeronautics and Space Administration
Washington, DC 20546–0001

10. SPONSORING/MONITORING AGENCY REPORT NUMBER

NASA TM—2003-212555

11. SUPPLEMENTARY NOTES

Responsible person, Narottam P. Bansal, organization code 5130, 216–433–3855.

12a. DISTRIBUTION/AVAILABILITY STATEMENT

Unclassified - Unlimited
Subject Categories: 07 and 27 Distribution: Nonstandard

Available electronically at http://gltrs.grc.nasa.gov

This publication is available from the NASA Center for AeroSpace Information, 301–621–0390.

12b. DISTRIBUTION CODE

13. ABSTRACT ***(Maximum 200 words)***

Celsian is a promising matrix material for fiber-reinforced composites for high temperature structural applications. Processing and fabrication of small diameter multifilament silicon carbide tow reinforced celsian matrix composites are described. Mechanical and microstructural properties of these composites at ambient and elevated temperatures are presented. Effects of high-temperature exposures in air on the mechanical behavior of these composites are also given. The composites show mechanical integrity up to ~1100 °C but degrade at higher temperatures in oxidizing atmospheres. A model has been proposed for the degradation of these composites in oxidizing atmospheres at high temperatures.

14. SUBJECT TERMS

Celsian; Barium aluminosilicate; Ceramic; Composites; Fibers; Mechanical properties; Silicon carbide

15. NUMBER OF PAGES

28

16. PRICE CODE

17. SECURITY CLASSIFICATION OF REPORT	18. SECURITY CLASSIFICATION OF THIS PAGE	19. SECURITY CLASSIFICATION OF ABSTRACT	20. LIMITATION OF ABSTRACT
Unclassified	Unclassified	Unclassified	